

# **Combining a hybrid chip and tube microfluidic system with fluorescent molecularly imprinted polymer (MIP) core-shell particles for the derivatisation, extraction and detection of peptides with N-terminating phosphorylated tyrosine**

Samual C. Burnage, Jérémy Bell, Wei Wan, Evgeniia Kislenco and Knut Rurack\*

*Bundesanstalt für Materialforschung und -prüfung (BAM), Richard-Willstätter-Str. 11, 12489 Berlin, Germany.*

**I. Synthesis of sensory particles M1**

**II. Micro-extractor parameters and designs**

**III. In-line derivatisation and ion exchange**

**IV. Analysis of peptides**

**V. State-of-the-art of MIP-based sensors for amino acid, peptide and protein detection**

**VI. References**

## I. Synthesis of sensory particles M1

Spherical, monodisperse, silica-core/fluorescent-MIP-shell particles **M1** were prepared as outlined in our previous work.<sup>1</sup> The silica core particles (SiO<sub>2</sub>, 320 nm) were prepared following a modified Stöber method. Ammonia solution (9.0 mL, 32%), absolute ethanol (16.3 mL) and Milli-Q water (24.8 mL) were mixed in a round-bottomed flask and stirred (1000 rpm). Subsequently, a mixture of tetraethyl orthosilicate (4.5 mL) and ethanol (45.5 mL) was added and further mixed (500 rpm) for 2 h. The obtained particles were washed with Milli-Q water and ethanol, then dried under vacuum overnight.

SiO<sub>2</sub> particles (1.0 g) and 3-aminopropyltriethoxysilane (APTES, 4.0 mL) were added to anhydrous toluene (56 mL). The mixture was heated under reflux for 12 h under argon. The resulting APTES-modified SiO<sub>2</sub> particles (NH<sub>2</sub>-SiO<sub>2</sub>) were separated by centrifugation, washed with toluene, and dried under vacuum.

The NH<sub>2</sub>-SiO<sub>2</sub> particles were subsequently coupled with a reversible addition-fragmentation chain-transfer (RAFT) agent. 4-Cyano-4-(thiobenzoylthio)pentanoic acid (822 mg, 2.95 mmol), ethylchloroformate (282 μL, 2.95 mmol) and triethyl amine (411 μL, 2.95 mmol) were added into a three-necked round-bottomed flask with anhydrous tetrahydrofuran (60 mL). The mixture was purged with argon and cooled to -78 °C for 40 min using an acetone-liquid nitrogen bath. NH<sub>2</sub>-SiO<sub>2</sub> (3.5 g) was cooled to -10 °C using a salt-ice bath and added to the mixture, where it was stirred at ambient temperature overnight. The obtained particles were precipitated in hexane (200 mL), washed with acetone, tetrahydrofuran and dried under vacuum overnight, resulting in RAFT modified SiO<sub>2</sub> core particles (RAFT-SiO<sub>2</sub>).<sup>2</sup>

The RAFT-SiO<sub>2</sub> particles (150 mg), methacrylamide (26.0 mg, 0.31 mmol), ethylene glycol dimethacrylate (284 mL, 1.51 mmol), crosslinker **1** (8.0 mg, 15.3 mmol), **Fmoc-pY-OEt.TBA** (11.5 mg, 15.3 mmol), and 4,4'-azobis(4-cyanovaleric acid) (8.7 mg, 35 mmol) were suspended and mixed in anhydrous chloroform (20 mL) and the mixture was then purged with argon. The subsequent mixture was polymerised at 50 °C for 18h, then further aged for 2 h at 70 °C. The synthesised particles were washed with acetonitrile and chloroform, dried under vacuum overnight resulting in silica core, **Fmoc-pY-OEt.TBA** imprinted polymer shell particles (**M1**). The non-imprinted polymer (NIP) control particles (**N1**) were synthesised under identical conditions but without the template.

## II. Micro-extractor parameters and designs

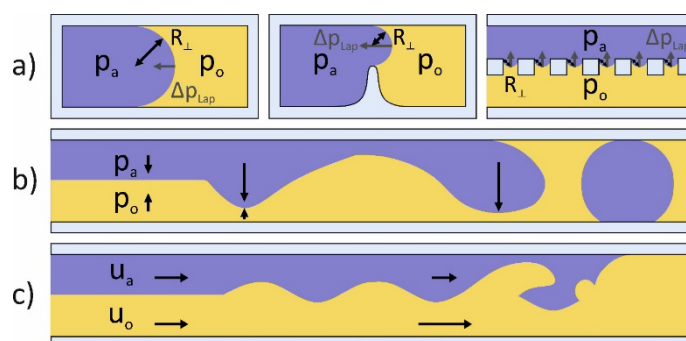


**Fig. S1.** a) Increasing Laplace stabilisation pressure from left to right. Left: Laplace pressure ( $\Delta p_{Lap}$ ) of two fluids flowing parallel to one another (flow into the plane of the paper), where  $R_{\perp}$  is the radius of the contact between the two phases,  $p$  is pressure,  $u$  is linear flow rate and subscripts **a** and **o** denote aqueous and organic respectively. Middle: Stabilising Laplace pressure in a three-dimensional guide extractor (flow into the plane of the paper). Right: Stabilising Laplace pressure in a micro-pillar extractor (flow left to right); b) Local pressure imbalance upon flowing two immiscible fluids parallel to one another; c) Kelvin-Helmholtz instability arising when two immiscible fluids flow at two different velocities. Aspects of these illustrations are based on the work of Xu and Xie.<sup>3</sup>

For the three-dimensional guide based micro-extractor, the limitations of the soft-lithography procedure were exploited by reducing the gap between two parallel channels below the resolution of the manufacturing process. The gap between the two channels was reduced to obtain a guide of 40  $\mu\text{m}$  height to stabilise the flows without reducing the interfacial surface area.

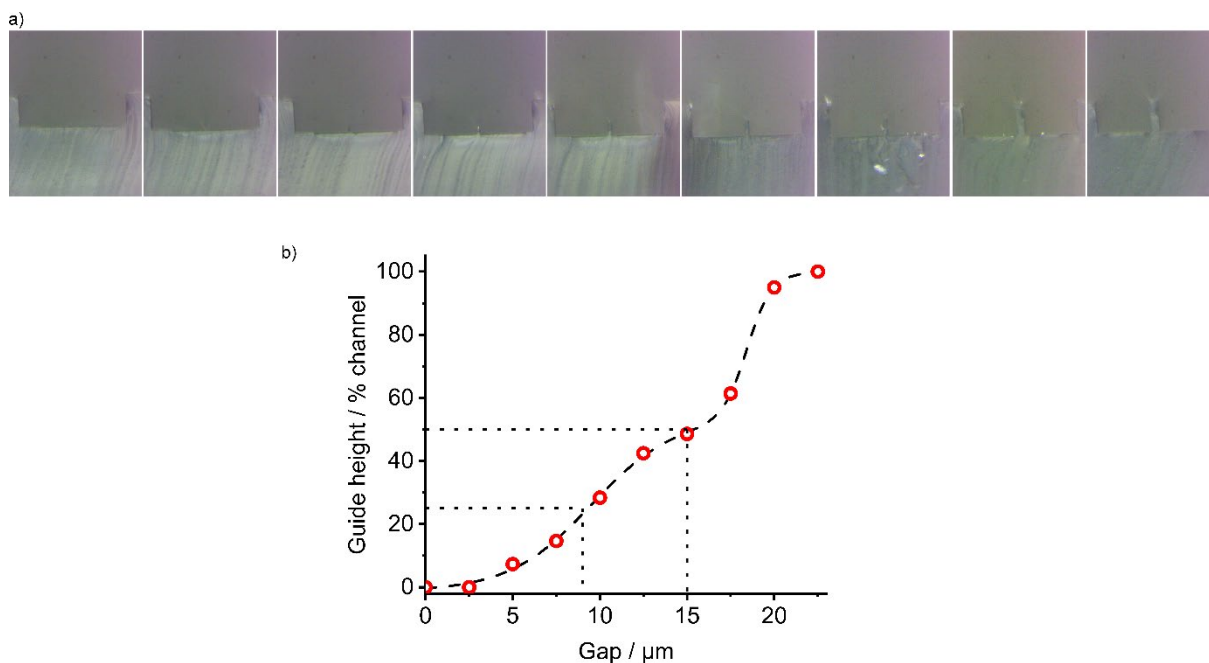


**Fig. S2.** a) Photographs of PDMS manufactured micro-extractor section upon increasing gap size between the two channels of the design, from left to right: 2.5, 5, 7.5, 10, 12.5, 15, 17.5, 20 and 22.5  $\mu\text{m}$ ; b) Respective plot of the guide height in per cent of the channel depth versus the gap size of the design.

The microfluidic chip was manufactured with PDMS (transparent or black) sealed on a microscope slide and presented a larger channel of 1 mm width for fluorescence analysis after the extractor unit. The micro-extractor consisted of two 30 mm long parallel channels of 200  $\mu\text{m}$  width separated by a guide (Figs. S3a, b) to ensure efficient extraction of the analyte. Such a configuration maximises mass transfer efficiency thanks to a large interface. The flow rates compatibility of chloroform and water phases was mapped to find the optimal combination of flow rates for this microchip design (Fig. S3c). According to this mapping, organic and aqueous phases had to be equilibrated to maintain stability and were set at the minimum stable flow rates of 7.5  $\mu\text{L min}^{-1}$  to ensure an extraction time of approximately 10 s.

Combining this microfluidic design with the previously described read-out system allowed detection of concentrations of **Fmoc-pY-OEt.TBA** from 5–50  $\mu\text{M}$  using both S2-1 and S2-2 with analysis errors of 5–10 % (Fig. S3d). In comparison to the monophasic assay, lower signal intensities were observed that can be attributed to incomplete extraction as well as interference from trace water, diminishing the strength of the hydrogen-bonding.

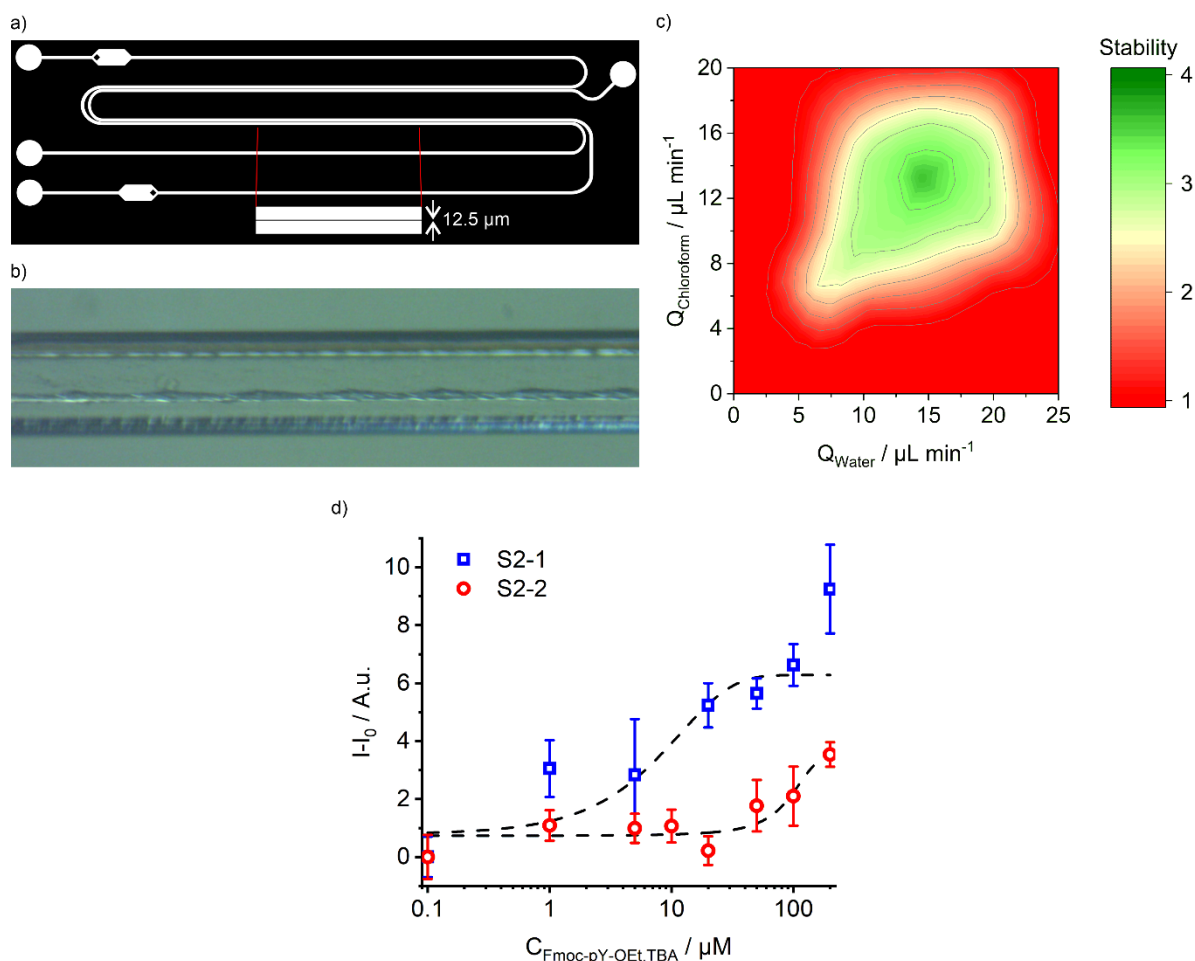


**Fig. S3.** a) Microchip design for **Fmoc-pY-OEt.TBA** extraction and detection with **M1** sensory particles with a central guide as an interface stabiliser; b) Microscope photograph of the micro-extractor with a central guide; c) Mapping of the guide micro-extractor stability versus water and chloroform solutions flows; d) Response of the two acquisition channels S2-1 (blue squares) and S2-2 (red circles) upon injection of increasing concentrations of **Fmoc-pY-OEt.TBA** in the aqueous phase and extraction and detection by the **M1** particles in the guide geometry extractor.

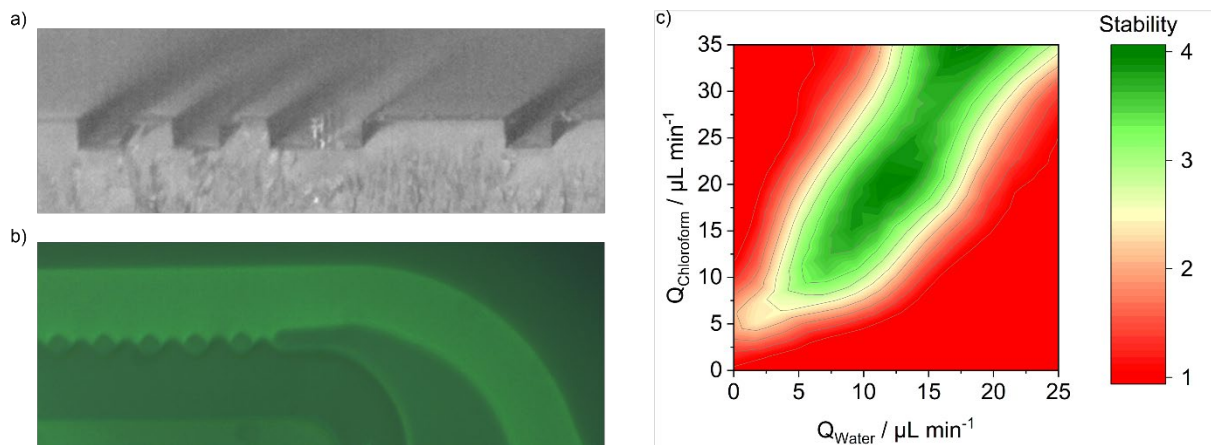


**Fig. S4.** a) Cross-sectional microscope photograph of the micro-extractor with micro-pillars along the centre a 100  $\mu\text{m}$  wide channel; b) Interface stability between dyed chloroform solution (top channel) and water (bottom channel) at the end of the micro-extractor; c) Mapping of the micro-pillars extractor stability versus water and chloroform solutions flow rate.

### III. In-line derivatisation and ion exchange

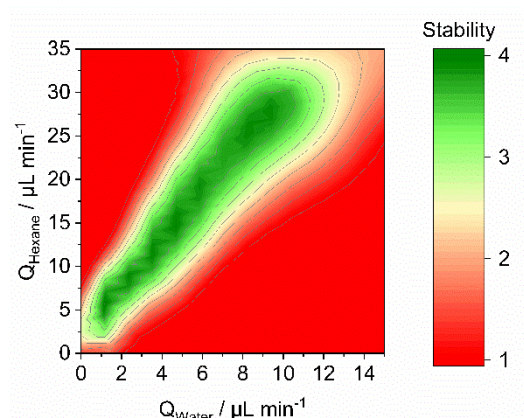


**Fig. S5.** Mapping of the micro-pillar extractor stability versus water and hexane flow rates.

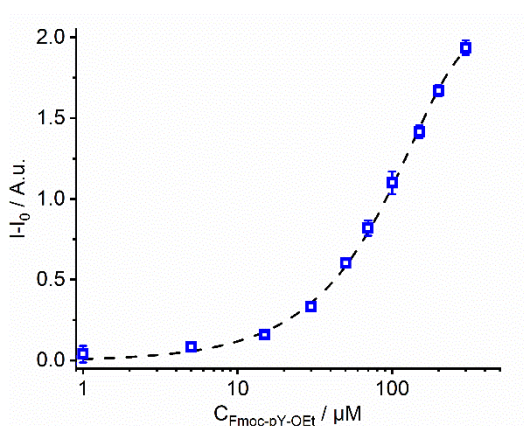


**Fig. S6.** Emission of the MIP sensory particles **M1** in chloroform phase (1 mL) upon addition of **Fmoc-pY-OEt** in the aqueous phase (1 mL) containing an excess of tetrabutylammonium hydroxide (TBA-OH, 10 mM) in a cuvette experiment.

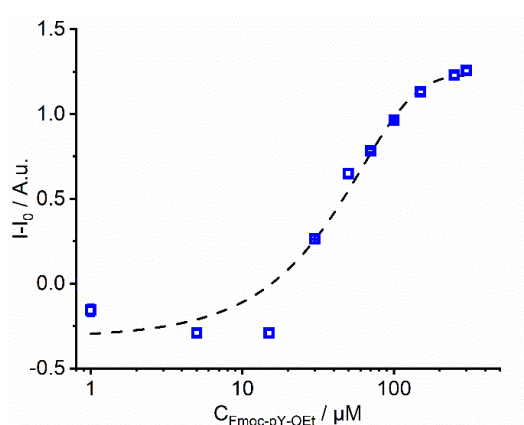


**Fig. S7.** Emission of the MIP sensory particles **M1** in chloroform phase (1 mL) containing an excess of tetrabutylammonium perchlorate (TBA- $\text{ClO}_4$ , 10 mM) upon addition of **Fmoc-pY-OEt** in the aqueous phase (1 mL) in a cuvette experiment.

#### IV. Analysis of peptides

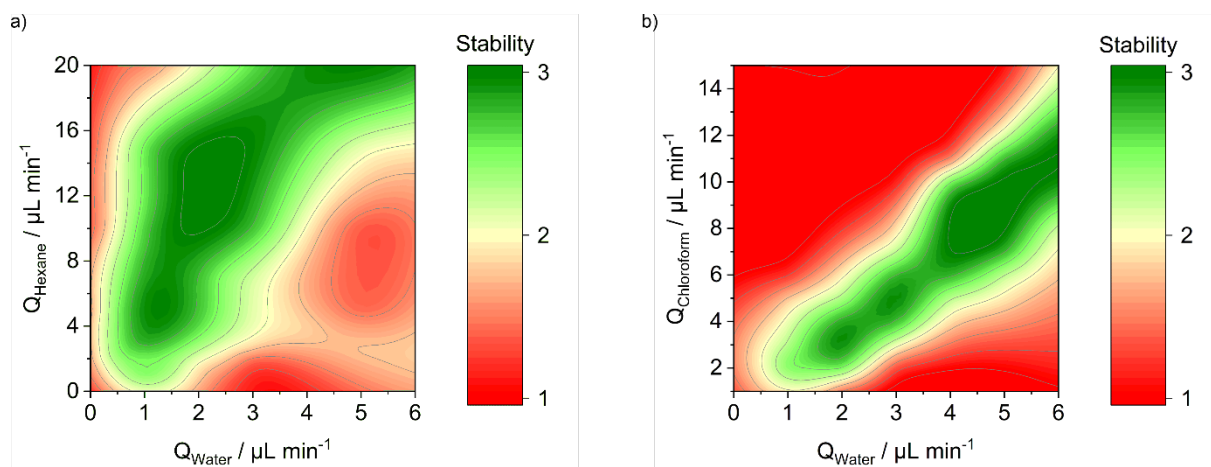


**Fig. S8.** a) Mapping of the micropillars micro-extractor stability versus water and hexane flow rates; b) Mapping of the micro-pillar extractor stability versus water and chloroform flow rates.

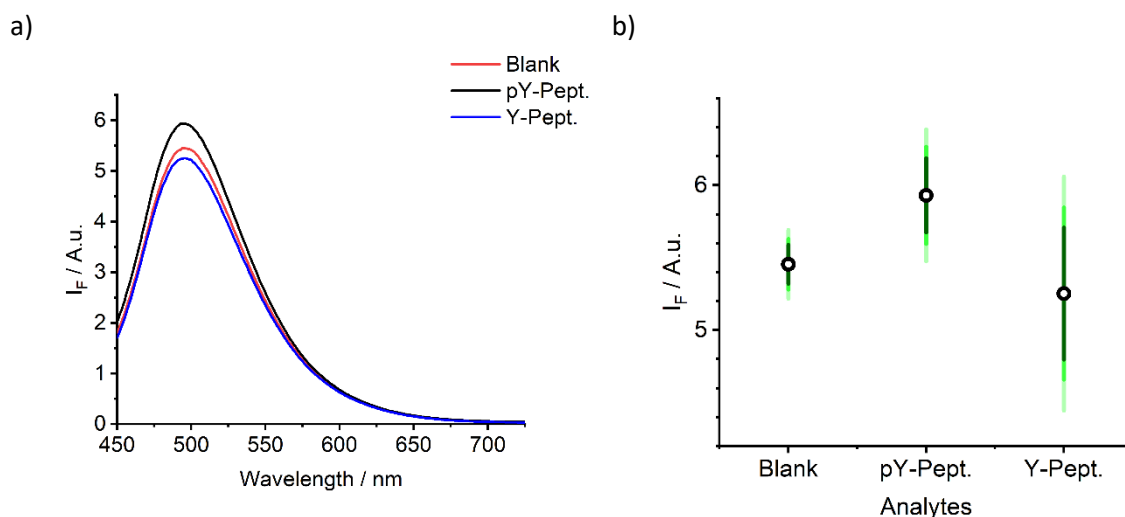


**Fig. S9.** Derivatization (Fmoc-Cl), ion-exchange (TBA-OH), extraction and detection of 25  $\mu\text{M}$  of **pY-Pept.** and **Y-Pept.** with MIP in biphasic cuvette assays. Emission of **M1** particles (a) and total relative uncertainties using various confidence intervals ( $t_{.80}$  dark green,  $t_{.85}$  medium green,  $t_{.90}$  light green). Total assay time of approx. 3 hours: solutions preparation, derivatization reaction (20 min) and workup, MIP extraction (1 min) including decantation after mixing (2 h), spectroscopic analyses (5 min).

## V. State-of-the-art of MIP-based sensors for amino acid, peptide and protein detection (n.r. = not reported)

No.	Year	Ref.	Analyte(s)	MIP material	Detection method	Working range	Limit of detection	Embedded platform	Assay time
1	2020	4	L-Tyrosine	MIP on gold nanoparticles and	Electrochemical	10 – 4000 nM	0.79 nM	no	n.r.
2	2020	5	Tyrosine phosphopeptide	MIP on quantum dots	Fluorescence	0.07 – 230 $\mu$ M	34 nM	no	n.r.
3	2022	6	L-Tryptophan	MIP-PVDF membrane	Surface Acoustic Wave	0.5 – 150 mg L <sup>-1</sup>	0.2 mg L <sup>-1</sup>	no	n.r.
4	2022	7	3-Nitrotyrosine, 4-Nitroquinolin-N-oxide	MIP on graphene quantum-dot	Electrochemical	0.005 – 500 $\mu$ M	≈ nM	Paper-based	n.r.
5	2021	8	L-Tyrosine	SERS-imprinted membrane	SERS	1 – 10 <sup>4</sup> nM	n.r.	no	n.r.
6	2022	9	L-Tyrosine	MIP-MOF	Fluorescence, luminescence	0.1 – 25 nM	80 pM	no	n.r.
7	2021	10	Vancromycin	Electropolymerized MIP	Electrochemical	0.17 – 2.0 $\mu$ M	n.r.	no	n.r.
8	2022	11	Interleukin 6	Electropolymerized MIP	Electrochemical	1 – 200 ng L <sup>-1</sup>	n.r.	no	n.r.
9	2022	12	GFNCRP (SARS-CoV-2 receptor binding domain)	Electropolymerized MIP	Electrochemical	10 – 50 nM	n.r.	no	n.r.
10	2022	13	Neutrophil gelatinase-associated lipocalin	Microcontact surface imprinting	Electrochemical	1 – 300 $\mu$ g L <sup>-1</sup>	n.r.	no	n.r.
11	2022	14	Human blood clotting factor IX protein	Aptamer-MIP	Electrochemical	n.r.	10.7 pM	no	n.r.
12	2020	15	Epitope of epidermal growth factor receptor	NanoMIP layer	thermistors	0 – 500 nM	10 nM	Thermistor cell	< 20 min
13	2019	16	Immunogenic gluten octamer epitope (PQQPPFQQ)	MIP film	Extended-gate field-effect	0.5 – 45 mg L <sup>-1</sup>	0.11 mg L <sup>-1</sup>	no	n.r.
14	2018	17	Neuron specific enolase	Electropolymerized MIP	Electrochemical	0.25 – 64 $\mu$ g L <sup>-1</sup>	n.r.	no	n.r.
15	2022	18	Dengue nonstructural protein 1	Electropolymerized MIP	Electrochemical	0.2 – 30 mg L <sup>-1</sup>	73 $\mu$ g L <sup>-1</sup>	no	n.r.
16	2021	19	Alpha-synuclein	MIP on conductive polymers	Electrochemical	n.r.	≈ pg L <sup>-1</sup>	no	n.r.
17	2022	20	IgG	MIP based on biopolymer	Surface Plasmon Resonance	n.r.	0.90 mg L <sup>-1</sup>	no	n.r.
18	2020	21	beta-Amyloid	MIP on carbon ink	Electrochemical	0.1 – 1000 $\mu$ g L <sup>-1</sup>	0.1 $\mu$ g L <sup>-1</sup>	Paper-based	20 min
19	-	<i>this study</i>	Phosphotyrosine, pY-Peptides	MIP on SiO <sub>2</sub> core	Fluorescence	1.5 – 50 $\mu$ M	1.5 $\mu$ M	Microfluidics	< 15 min

## VI. References

1. W. Wan, A. B. Descalzo, S. Shinde, H. Weisshoff, G. Orellana, B. Sellergren and K. Rurack, *Chem. Eur. J.*, **2017**, *23*, 15974–15983.
2. W. Wan, M. Biyikal, R. Wagner, B. Sellergren and K. Rurack, *Angew. Chem. Int. Ed.*, **2013**, *52*, 7023–7027.
3. C. Xu and T. Xie, *Ind. Eng. Chem. Res.*, **2017**, *56*, 7593–7622.
4. B. J. Chen, Y. S. Zhang, L. Lin, H. Chen and M. J. Zhao, *J. Electroanal. Chem.*, **2020**, *863*, 114052.
5. N. S. Amiri and M. R. M. Hosseini, *Anal. Methods*, **2020**, *12*, 63–72.
6. K. Prabakaran, P. J. Jandas, J. T. Luo and C. Fu, *Sens. Actuators, A*, **2022**, *341*, 113525.
7. M. Amatongchai, N. Nontawong, P. Ngaosri, S. Chunta, S. Wanram, P. Jarujamrus, D. Nacapricha and P. A. Lieberzeit, *Anal. Chem.*, **2022**, *94*, 16692–16700.
8. H. Li, Y. Li, D. Wang, J. Wang, J. Zhang, W. Jiang, T. Zhou, C. Liu and G. Che, *Sens. Actuators, B*, **2021**, *340*, 129955.
9. S. Tang, P. Zhao, X. Wu, Y. Chen, K. Tang, S. Zhou, J. Fu, H. Lei, Z. Yang and Z. Zhang, *Sens. Actuators, B*, **2022**, *367*, 132058.
10. F. Tan, M. Y. Zhai, X. J. Meng, Y. Wang, H. X. Zhao and X. C. Wang, *Biosens. Bioelectron.*, **2021**, *184*, 113220.
11. Y. T. Yaman, O. A. Vural, G. Bolat and S. Abaci, *Bioelectrochemistry*, **2022**, *145*, 108053.
12. X. R. Zhang, A. T. Waffo, A. Yarman, N. Kovacs, Z. Bognar, U. Wollenberger, I. M. El-Sherbiny, R. Y. A. Hassan, F. F. Bier, R. E. Gyurcsanyi, I. Zebger and F. W. Scheller, *Nanoscale*, **2022**, *14*, 18106–18114.
13. J. C. Yang, C. H. Cho, D. Y. Choi, J. P. Park and J. Park, *Sens. Actuators, B*, **2022**, *364*, 131916.
14. H. Krishnan, S. C. B. Gopinath, M. K. M. Arshad, H. I. Zulhaimi, P. Anbu and S. Subramaniam, *Sens. Actuators, B*, **2022**, *363*, 131842.
15. K. Betlem, F. Canfarotta, R. Raumbault, C. E. Banks, K. Eersels, B. van Grinsven, T. J. Cleij, R. Crapnell, A. Hudson and M. Peeters, *Analyst*, **2020**, *145*, 5419–5424.
16. Z. Iskierko, P. S. Sharma, K. R. Noworyta, P. Borowicz, M. Cieplak, W. Kutner and A. M. Bossi, *Anal. Chem.*, **2019**, *91*, 4537–4543.
17. R. Tchinda, A. Tutsch, B. Schmid, R. D. Sussmuth and Z. Altintas, *Biosens. Bioelectron.*, **2019**, *123*, 260–268.
18. C. E. Buensuceso, B. D. B. Tiu, L. P. Lee, P. M. G. Sabido, G. M. Nuesca, E. B. Caldon, F. R. del Mundo and R. C. Advincula, *Anal. Bioanal. Chem.*, **2022**, *414*, 1347–1357.
19. M. H. Lee, J. L. Thomas, Z. L. Su, W. K. Yeh, A. S. Monzel, S. Bolognin, J. C. Schwamborn, C. H. Yang and H. Y. Lin, *Biosens. Bioelectron.*, **2021**, *175*, 112852.
20. F. Torrini, F. Battaglia, P. Palladino, S. Scarano and M. Minunni, *Biosens. Bioelectron.*, **2022**, *217*, 114706.
21. M. V. Pereira, A. C. Marques, D. Oliveira, R. Martins, F. T. C. Moreira, M. G. F. Sales and E. Fortunato, *ACS Omega*, **2020**, *5*, 12057–12066.